Journal of Coastal Research	24	6	1418–1429	West Palm Beach, Florida	November 2008

Utilizing Spectral Analysis of Coastal Discharge Computed by a Numerical Model to Determine Boundary Influence

Eric D. Swain[†], Christian D. Langevin[†], and John D. Wang[‡]

[†]U.S. Geological Survey
Florida Integrated Science Center
3110 SW 9th Avenue
Fort Lauderdale, FL 33315, U.S.A.
edswain@usgs.gov

[‡]Rosenstiel School of Marine and Atmospheric Science
University of Miami
4600 Rickenbacker Causeway
Miami, FL 33149-1098, U.S.A.

ABSTRACT

SWAIN, E.D.; LANGEVIN, C.D., and WANG, J.D., 2008. Utilizing spectral analysis of coastal discharge computed by a numerical model to determine boundary influence. *Journal of Coastal Research,* 24(6), 1418–1429. West Palm Beach (Florida), ISSN 0749-0208.

In the present study, a spectral analysis was applied to field data and a numerical model of southeastern Everglades and northeastern Florida Bay that involved computing and comparing the power spectrum of simulated and measured flows at the primary coastal outflow creek. Four dominant power frequencies, corresponding to the S1, S2, M2, and O1 tidal periods, were apparent in the measured outflows. The model seemed to reproduce the magnitudes of the S1 and S2 components better than those of the M2 and O1 components. To determine the cause of the relatively poor representation of the M2 and O1 components, we created a steady-base version of the model by setting the time-varying forcing functions—rainfall, evapotranspiration, wind, and inland and tidal boundary conditions—to averaged values. The steady-base model was then modified to produce multiple simulations with only one time-varying forcing function for each model run. These experimental simulations approximated the individual effects of each forcing function on the system.

The spectral analysis of the experimental simulations indicated that temporal fluctuations in rainfall, evapotranspiration, and inland water level and discharge boundaries have negligible effects on coastal creek flow fluctuations with periods of less than 48 hours. The tidal boundary seems to be the only forcing function inducing the M2 and O1 frequency flow fluctuations in the creek. An analytical formulation was developed, relating the errors induced by the tidal water-level gauge resolution to the errors in the simulated discharge fluctuations at the coastal creek. This formulation yielded a discharge-fluctuation error similar in magnitude to the errors observed when comparing the spectrum of the simulated and measured discharge. The dominant source of error in the simulation of discharge fluctuation magnitude is most likely the resolution of the water-level gauges used to create the model boundary.

ADDITIONAL INDEX WORDS: *Fourier transform, model boundary, tidal forcing, frequency domain, gauge error.*

INTRODUCTION

The southern inland and coastal systems (SICS) numerical flow model was developed for the coastal area of Everglades National Park and Florida Bay in southern Florida (Figure 1). The flow volumes and patterns of flow through the coastal creeks connecting the inland and offshore areas are of great interest to water managers and others implementing ecosystem restoration initiatives. Surface water is represented in the SICS model by SWIFT2D—a two-dimensional hydrodynamic model capable of simulating constituent transport and density variations (SCHAFFRANEK, 2004). It is coupled to SEAWAT, the three-dimensional groundwater model (GUO and LANGEVIN, 2002), which has comparable transport and density variation capabilities. Applying the coupled model to the SICS area required adding further capabilities to represent evapotranspiration, rainfall, and wind sheltering (SWAIN *et al.,* 2004). The calibration of the SICS model was complex, owing to many parameters (LANGEVIN, SWAIN, and WOLFERT, 2005). The properties of measured and simulated values were compared to ensure proper model development and calibration.

A coupled surface-water–groundwater model was needed for the SICS area because of significant interactions between the coastal wetlands and the aquifer. The capability to represent the density effects of constituent transport is needed because of the coastal salinity gradient, and the hydrodynamic surface-water solution is required to accurately simulate the coastal stage and flow transients. The necessary complexity of this scheme also means that the model needs much more input data than simpler models, requires greater development effort, and has more sources of uncertainty. To place error bounds on model results, we had to determine the sources of error in the extensive input data.

The results of the numerical model can be compared with field measurements for calibration. In the SICS model area, water levels, salinity, and discharge rates are measured at the coastal creeks where flow exits the wetlands into Florida Bay. A comparison of the magnitude and frequency of fluctuations in each data set can be useful, providing insight as

DOI: 10.2112/07-0848.1 received 9 March 2007; accepted in revision 18 July 2007.

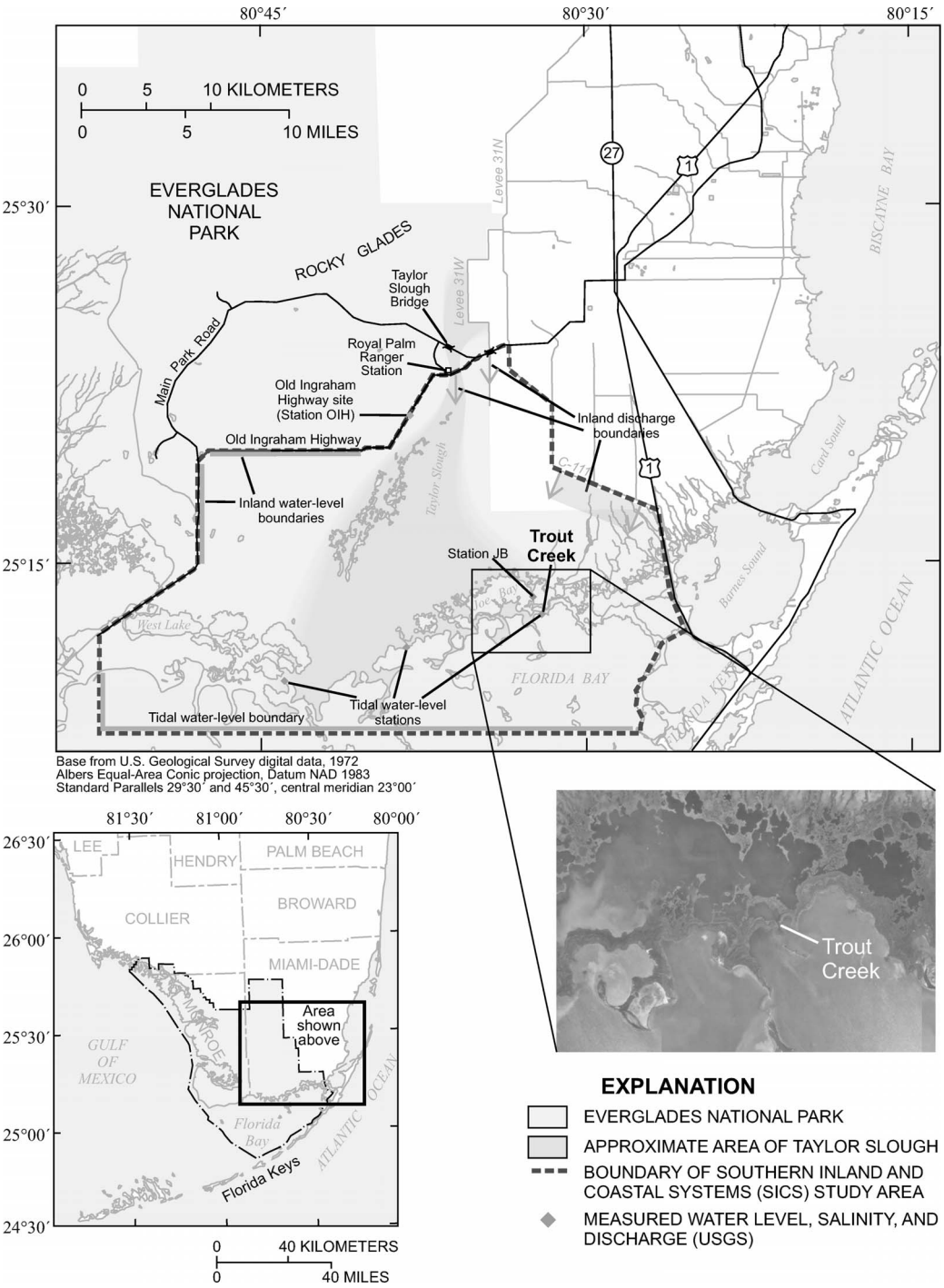

Figure 1. Southern Inland and Coastal Systems (SICS) study area.

to which factors drive the flows. The dominant frequencies in both measured and simulated data can be delineated by spectral analysis in which data are transformed into a frequency domain that represents the distribution of fluctuation amplitudes. These dominant frequencies can then be compared to evaluate the ability of the numerical model to represent the relevant controlling phenomena. The input parameters can be varied to identify those factors that are manifested at each of the dominant frequencies. It is also possible to determine the spectral amplitude at specific frequencies, which indicates the magnitude of the effects. Through the combination of a numerical model and spectral analysis, the dominant

forcing functions of the system can be identified and the ability of the model to reproduce the effects of the forcing functions can be evaluated.

NUMERICAL MODELING AND SPECTRAL ANALYSIS

The development of the SICS numerical model has involved numerous field studies to define model input, such as frictional resistance, evapotranspiration, land elevation, boundary conditions, and other parameters (SCHAFFRANEK, RUHL, and HANSLER, 1999). HITTLE (2000) installed coastal monitoring sites at several locations, including Trout Creek, shown in Figure 1. The water-level, discharge, and salinity data (collected at 15-minute intervals) at this site and others are used to calibrate the model.

The model represents predominant downward flow of surface water to groundwater at the coastline, with upwelling offshore. However, the model shows coastal groundwater fluxes to be small relative to surface-water fluxes (LANGEVIN, SWAIN, and WOLFERT, 2005), and the focus of this report is on the surface-water component as a more significant measure of model hydrology. A simulation timestep of 3 minutes is used in SWIFT2D, whereas boundary conditions are input at different timestep lengths. Evapotranspiration is computed every timestep, but the solar-radiation values used to compute evapotranspiration are input every 15 minutes. Rainfall, wind, and tidal boundaries are also input at 15-minutes intervals.

The tidal boundary is computed as an average of the three tidal water-level stations shown in Figure 1. Rainfall is spatially interpolated between rainfall stations and wind speed, and direction is spatially uniform over the model area. Solar radiation is spatially uniform but evapotranspiration varies between model cells because of its dependence on water depth and vegetation. The spatial and temporal resolution of the model should be sufficient to examine fluctuations in flow rates on scales somewhat larger than the computational timestep.

A useful tool to investigate and compare the properties of both the water-level and discharge fluctuations is spectral analysis, in which the Fourier transform of the autocovariance function is defined as the spectrum (LUMLEY and PANOFSKY, 1964):

$$S_{xx}(\omega) = \frac{1}{2\pi} \int_{-\infty}^{\infty} e^{i\omega\tau} C_x(\tau)\, d\tau \qquad (1)$$

where $S_{xx}(\omega)$ is the spectrum of quantity $x(t)$ at a time frequency of ω, i is the imaginary number $\sqrt{-1}$, and $C_x(\tau)$ is the autocovariance of quantity x at a time lag of τ computed by:

$$C_x(\tau) = \frac{1}{T} \int_0^T [x(t) - \bar{x}][x(t + \tau) - \bar{x}]\, dt \qquad (2)$$

where t is time, T is the total time analyzed, and $\bar{x}$ is the time-averaged value of quantity $x(t)$ over time T. The spectrum expresses the magnitude of correlations in the x values at frequency ω. The implementation of spectral analysis is facilitated by the use of a fast-Fourier transform (FFT) technique (COOLEY and TUKEY, 1965). This discrete Fourier-transform algorithm reduces the number of computations needed and efficiently calculates the spectral power distribution.

Various studies have used spectral analysis or associated stochastic techniques on model results. RETTEMEIER *et al.* (2001) used a spectral analysis on results from a finite-element model of flow and turbulence in which a comparison was made between theoretical distributions and frequency spectra of three-dimensional turbulence at a node in the model. SHIH (2004) used differential analysis to create analytic statistical formulations for uncertainty analysis. These formulations were utilized on a radioactive nuclide transport model. In another study, FERRANTE and YEH (1999) used spectral analysis and Monte Carlo simulations to propagate uncertainty into simulated flow through unsaturated soils. SWAIN and CHIN (2003) used spectral integration to develop an analytical formulation of dispersion in groundwater affected by variable surficial recharge. Although application of spectral analysis indicates the ability of a model to represent a system, the study described in this paper also employed a spectral analysis on model output to determine the significance of model boundaries. This analysis yields much more information about the behavior of the system than would have been possible from only comparing model results to field measurements.

Characteristic frequencies of the fluctuations in water level and discharge rate are caused by numerous factors, such as tides at coastal locations. The principal tidal components are listed in Table 1; in many offshore and estuary studies, these tidal components represent the majority of effects. Processes such as rainfall, wind, and evapotranspiration, however, have their own characteristic frequencies. Comparison of the spectra of forcing functions (such as tide and atmospheric pressure) and the spectral of water-level responses has been useful in determining their relationships (SHIH *et al.,* 2000), so a similar application can yield insight into the factors that affect coastal discharge. Determining which processes are manifested at a given frequency can be difficult, but the numerical model allows processes to be modified or neglected as specified so that their individual effects on model output can be estimated.

Application

The SICS study area consists of about 905 km² of southeastern Everglades National Park and includes part of northeastern Florida Bay and its shoreline from U.S. Highway 1 westward about 48 km to the West Lake area (Figure 1). The study area boundary then follows part of the Old Ingraham Highway northeastward to the Taylor Slough Bridge Royal Palm Ranger Station, and then southeastward along part of the C-111 canal. In addition to Taylor Slough, this area also includes several coastal creeks and several shallow coastal embayments such as Joe Bay. The SICS model was implemented to simulate a period from 1996 to 2002. Boundary conditions were constructed from measured discharges on the northern side of the model and measured water levels for the tidal boundary on the southern side. The calibrated model

Table 1. *Tidal frequency components (compiled from Schureman, 1976).*

Component	Period				Description
	Days	Hours	Minutes	Seconds	
K1	0	23	56	3	Lunisolar diurnal constituent. Together with O1, it expresses the effect of the moon's declination, which accounts for diurnal inequality and extreme diurnal tides. With P1, it expresses the effects of the sun's declination.
K2	0	11	58	2	Lunisolar semidiurnal constituent. Modulates the amplitude and frequency of M2 and S2 for the declinational effects of the moon and sun, respectively.
M1	1	0	50	28	Smaller lunar elliptic diurnal constituent.
M2	0	12	25	14	Principal lunar semidiurnal constituent. Represents the rotation of the Earth with respect to the moon.
N2	0	12	39	30	Larger lunar elliptic semidiurnal constituent. Together with L2, it modifies the amplitude and frequency of M2 for the effects of variation in the moon's orbital speed due to its elliptical orbit.
O1	1	1	49	9	Lunisolar diurnal constituent. See K1.
P1	1	0	3	57	Solar diurnal constituent. See K1.
S1	1	0	0	0	Principal solar diurnal constituent.
S2	0	12	0	0	Principal solar semidiurnal constituent. Represents the rotation of the Earth with respect to the sun.

output includes stage and discharge at the coastal creeks; these quantities also are measured in the field.

Trout Creek provides the largest volume of coastal creek output (Figure 1), and therefore, was chosen to compare spectral analysis of measured and simulated values. Figure 2 shows the discharge at Trout Creek and the tidal water level over a several-day period. The standard diurnal tides are not readily visible because the sheltering effect of the Florida Keys somewhat isolates Florida Bay (Figure 1). This makes the definition of fluctuation frequencies more difficult.

To ensure that nonstationary effects did not play a significant part in the spectral analysis, the Trout flow datasets were detrended and each split into multiple segments, and the spectral analysis performed on each segment, with the results averaged, similar to SHIH (2002) and SHIH and LIN (2002). The segment lengths were varied to find a good value; using more segments caused some of the significant frequency features to be lost. A segment length of about 450 days was chosen. The results of the spectral analysis of Trout Creek discharge (both measured and computed by the calibrated model) are shown in Figure 3 as a periodogram, where the abscissa is dimensioned in the inverse of frequency, which is the period length. Only periods of less than 48 hours are plotted because shorter timescale fluctuations are a better indicator of model uncertainty. Spectral power is greatest at several dominant frequencies (Figure 3). The 12-hour cycle corresponds to the S2 tidal component, the 12-hour 25-minute cycle corresponds to the M2 component, the 24-hour cycle corresponds to the S1 component, and the 1-day, 1-hour, 49-minute cycle corresponds to the O1 component. However, it should not be assumed that these components are strictly astronomical tides. The geography of northeastern Florida Bay shelters the coastal area and significantly dampens the tidal signature so frequency components observed as the S1 and S2 can easily be due to the other forcing functions such as wind, rain, or evapotranspiration.

The 95% confidence limits for the spectra indicate the sig-

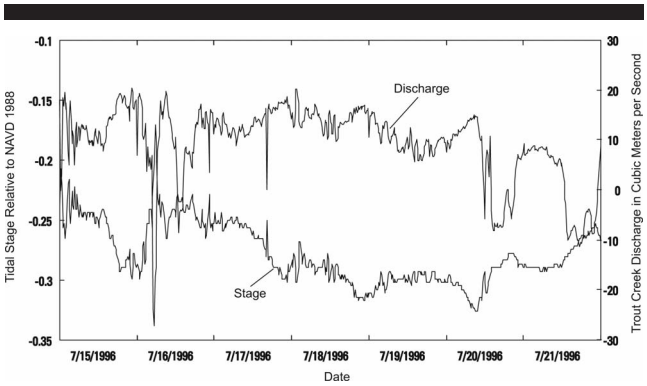

Figure 2. Trout Creek discharge and tidal water-level.

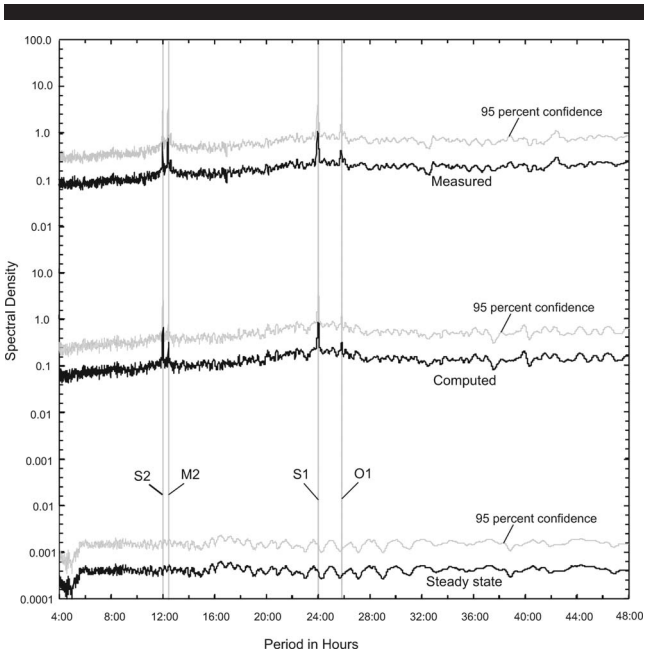

Figure 3. Periodograms of discharge conditions at Trout Creek.

nificance of spectral power (SHIH, 2002) and are calculated as per BENDAT and PIERSOL (2000):

$$\frac{2nS_{xx}}{\chi^2_{2n;0.025}} \leq S_{xx} \leq \frac{2nS_{xx}}{\chi^2_{2n;0.975}} \quad (3)$$

where n is the number of segments used and χ^2 is the chi-squared distribution value for the given degrees of freedom and percentage. The upper limit is plotted in Figure 3. The confidence limit lies above the spectral power at each frequency, but it is useful to see how the peaks in power compare with the mean 95% confidence line. The S2, M2, and S1 spectral power are above the mean confidence line for the measured data, but the M2 power falls significantly below in the case of the model computed data. The O1 component is lower than the mean confidence line in both cases.

The comparison of measured and simulated spectra (Figure 3) indicates how well the model reproduces the proper amplitude at the different frequencies. When comparing the magnitude of the dominant spectral power, the calibrated model reproduces 83% of the 12-hour component, 36% of the 12-hour 25-minute component, 85% of the 24-hour component, and 76% of the 1-day, 1-hour, 49-minute component (Table 2). The model seems to reproduce the 12- and 24-hour components (S2 and S1) better than the 12-hour, 25-minute and 1-day, 1-hour, 49-minute components (M2 and O1). To evaluate sources of model error, we varied the model forcing functions individually; determining the sources of these spectral components of flow.

Spectral Analysis of Experimental Simulations

To create a "steady-base" scenario without the effects of forcing-function fluctuations, the water-level, discharge, and salinity boundaries for the surface-water model and the water-level and salinity boundaries for the groundwater model were set to a constant value equal to the average for the 7-year simulation. This steady-base case, however, cannot be considered an actual average of the hydrology of the dynamic model because so many of the processes are nonlinear. When the fluctuations of a single-forcing function are added internal to the experimental simulations, the frequency and amplitude of their effects on coastal flows at Trout Creek can be determined by spectral analysis of the model output.

The spectral analysis of the simulation with constant surface-water and groundwater boundaries is shown along with the original simulation in Figure 3. For this first experimental situation, no significant spectral power is seen in the range of periods up to 48 hours, and none of the tidal frequencies is apparent (Figure 3).

When evaluating the spectral power peaks for single-forcing function simulations, their magnitudes can be compared with the equivalent spectral power of the field-measured data. However, this does not give an absolute measure of the percentage of the signal accounted for by each forcing function. The single forcing-function simulations do not take into account interactions between forcing functions, and the peak value of a spectral power is affected by how much lateral spread the peak has. Thus the real significance of applying forcing functions individually and comparing their spectral

Table 2. *Spectral power of Trout Creek discharge at principal tidal periods (determined from maximum value on periodogram; all data and model periods are 7 years in length).*

Variable or Model	Data Type and Origin	Measurement Error	Measurement Timestep	Standard Deviation of Data	Spectral Power as Percentage of Value In Field-Measured Data (Dashes Indicate Negligible Power)			
					12-h, 25-min Component (M2)	25-h, 49-min Component (O1)	12-h Component (S2)	24-h Component (S1)
Calibrated model using all forcing functions					36	76	83	85
Evapotranspiration	Computed from solar radiation collected at station OIH (Figure 1) (German, 2000)	For solar radiation, LI-200 pyranometer error <5%	15 min	287.0 W/m^2	—	—	—	5
Wind	Friction computed from wind velocity collected at station JB (Figure 1) (Jenter, 1999)	Model 05305 anemometer error <0.2 m/s	15 min	2.26 m/s	—	—	71	75
Tidal boundary	Tidal water-level stations (Figure 1) (Hittle, 2000)	±0.15 cm	15 min	10.1 cm	48	95	44	40

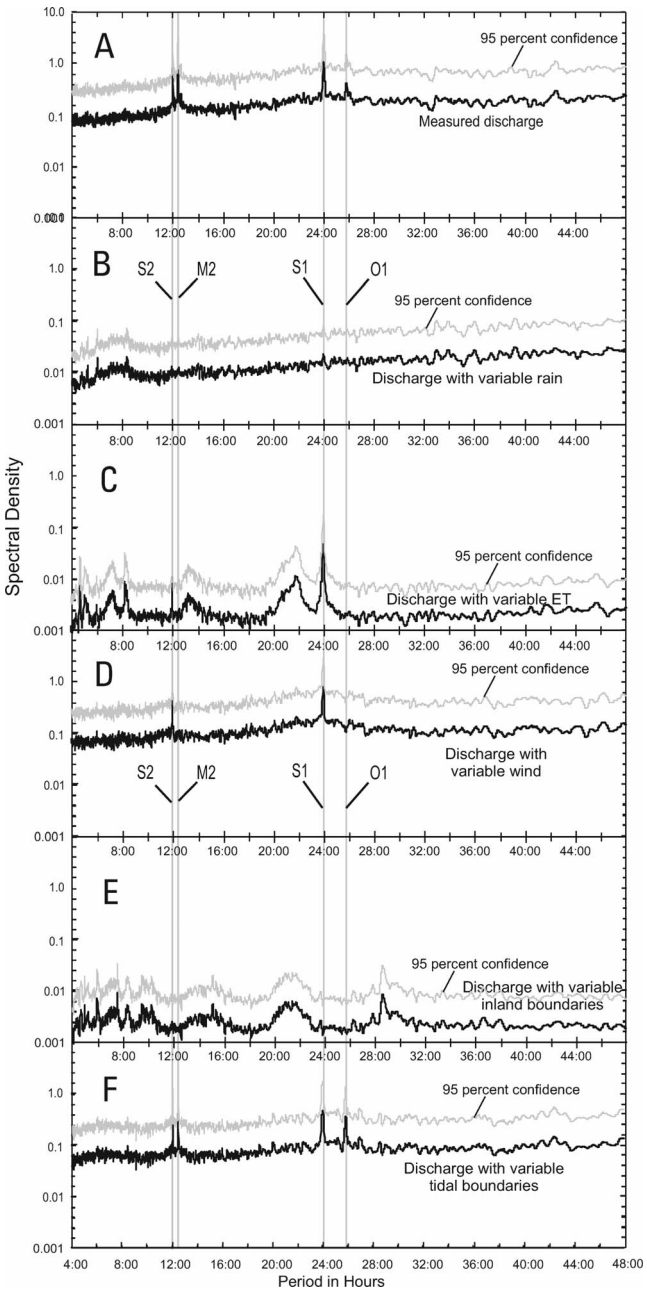

Figure 4. Periodograms of discharge conditions at Trout Creek with individual forcing functions.

magnitudes is to determine which forcing function the fluctuation in Trout Creek flow is most sensitive to, rather than strictly comparing the spectral magnitudes.

A spectral analysis of experimental simulations was made in which rainfall, evapotranspiration, wind, and inland and tidal boundaries were individually varied while other variables were held constant. In the first case, the actual rainfall time series was used, but all other input data remained constant at their average values. As shown in Figure 4B, no distinctive dominant spectral power was present within the range of frequency periods up to 48 hours. This can be compared with the spectra of the measured data in Figure 4A. The response of Trout Creek discharge to a rainfall event should depend on the "time of concentration"; the time it takes the water to flow from the furthest point in the watershed to Trout Creek. With mean flow velocities on the order of 1 cm/s, and distances more than 20 km, it can take over 20 days for rainwater to reach the coastal creeks. Although peak flows would occur in a shorter time, it makes sense that the discharge response would not be on the same timescale as the rainfall event. The spectral power magnitude gradually increased with longer period length, which indicates that the temporal variation in rainfall is dampened by the system as it flows to Trout Creek.

A similar damping as seen in the response to rainfall should occur with the evapotranspiration signal, but the strength of the daily evapotranspiration cycle is larger than that of the rainfall. A spectral analysis of the simulation in which only the evapotranspiration boundary was varied (Figure 4C) showed very little spectral power for most of the frequency periods. A small increase in spectral power occurred at the 24-hour period; however, this daily frequency in evapotranspiration was anticipated. The magnitude of this spectral power was 5% of the magnitude of the 24-hour spectral power seen in the field-measured data in Figure 4A (Table 2). This indicates that a very small part of the 24-hour response in Trout Creek flows is due to evapotranspiration variation. This contrasts with rainfall, which contributes a majority of the volumetric flow, but does not produce even a small 24-hour spectral power as does evapotranspiration. The spectral power from rainfall is highly muted because the discharge from a day's rainfall drains through the creeks over several days. Evapotranspiration fluctuates daily and peaks nearly simultaneously everywhere.

In a spectral analysis of flow at Trout Creek in which only the wind boundary was varied, spectral power is seen for both the 12- and 24-hour cycles (Figure 4D). Significant spectral energy was distributed more uniformly across all the frequencies, indicating that wind has a greater randomly distributed effect on high frequency flow variations than rainfall or evapotranspiration. The 12- and 24-hour spectral power in the wind-only spectrum were significant relative to the magnitude of the corresponding spectral power for the field-measured data spectrum (Table 2). This indicates that local wind forcing can be a significant factor in Trout Creek flow fluctuations at the frequency of the S1 and S2 components of tide. The significance of wind on coastal creek flow was also observed in SWAIN *et al.* (2004), where it is shown that the SICS model represents the periodic reversals of flow direction at Trout Creek. However, when the wind forcing is removed from the model, no flows in the inland direction are simulated so the significance of wind in the spectral analysis is not surprising.

The inland boundaries are defined as those not directly affected by the tidal variations from Florida Bay (Figure 1). This includes water levels along Old Ingraham Highway and flow through the Taylor Slough Bridge, L-31W Canal, and C-111 Canal (Figure 1). An analysis was made in which the spectrum of flow at Trout Creek with inland boundaries alone

was varied (Figure 4E). Minimal spectral energy was demonstrated in frequencies with periods less than 48 hours.

The only remaining forcing function, the tidal boundaries, was varied in the model, and dominant spectral power was seen at the S1, O1, S2, and M2 frequencies (Figure 4F). The 12- and 24-hour spectral power was not as large in magnitude as that generated when only the wind boundary was varied, but the 12-hour, 25-minute component (M2) and the 1-day, 1-hiyr, 49-minute component (O1) were significant with variable tidal boundaries. These peaks were not present in the spectral analysis of wind. This result is logical because the O1 and M2 frequencies are strictly lunar and lunisolar tidal components (Table 1).

A summary of the comparative magnitude of the power spectra is shown in Table 2. Comparing the calibrated model to the field-measured flow data at Trout Creek, the 24- and 12-hour frequencies (S1 and S2, respectively) are represented significantly better than the 12-hour, 25-minute (M2) and somewhat better than the 25-hour, 49-minute (O1) frequencies. The comparisons of the individual forcing-function simulations indicate that the 12-hour, 25-minute (M2) and 25-hour, 49-minute (O1) components are most likely induced exclusively by the tidal boundary. Additionally, wind may induce more of the 24- and 12-hour components (S1 and S2) than is induced by the tidal boundary. That the tidal boundary data include regional effects of wind, in addition to the S1 and S2 components, reinforces the conclusion that the S1 and S2 components, which represent solar tidal effects, do not seem to be as large an effect as the 24- and 12-hour spectral components of wind.

Additional insight can be obtained by directly comparing the forcing functions that are input to the model to the field flow data that the model is attempting to reproduce. This model-independent comparison uses the normalized cross-spectrum—the coherence. This indicates the correlation between data sets at specific spectral frequencies. The same partitioning of the data into segments (SHIH *et al.,* 2000) is used as in the spectral analysis. Figure 5A indicates that tidal level and Trout Creek flow have higher coherence at all four tidal frequencies, whereas Figure 5B shows wind and Trout Creek flow only have higher coherence at the S1 and S2 frequencies. This supports the conclusion that the indicated S1 and S2 frequencies are not predominantly astronomical tides but are wind driven. A comparison of Figures 5A and B indicates that the Trout Creek flow has a higher coherence with tide than wind over most of the frequency range, but at the S1 and S2 frequencies, neither tide nor wind can be proven to be a dominant effect. Figure 5C compares tide and wind, showing a higher coherence at the S1 and S2 frequencies. Because the boundary tidal level is affected by wind, very little of the observed S1 and S2 coastal flow fluctuations may be due to astronomical tides.

The S1 and S2 frequency effects on flow at Trout Creek seem to be primarily wind driven, and the M2 and O1 frequencies seem to be induced by the tidal boundaries. This result provides insight on how accurately these forcing functions are represented in the model.

Several conclusions can be drawn from the data presented in Table 2 and Figures 3–5: The effects of evapotranspiration

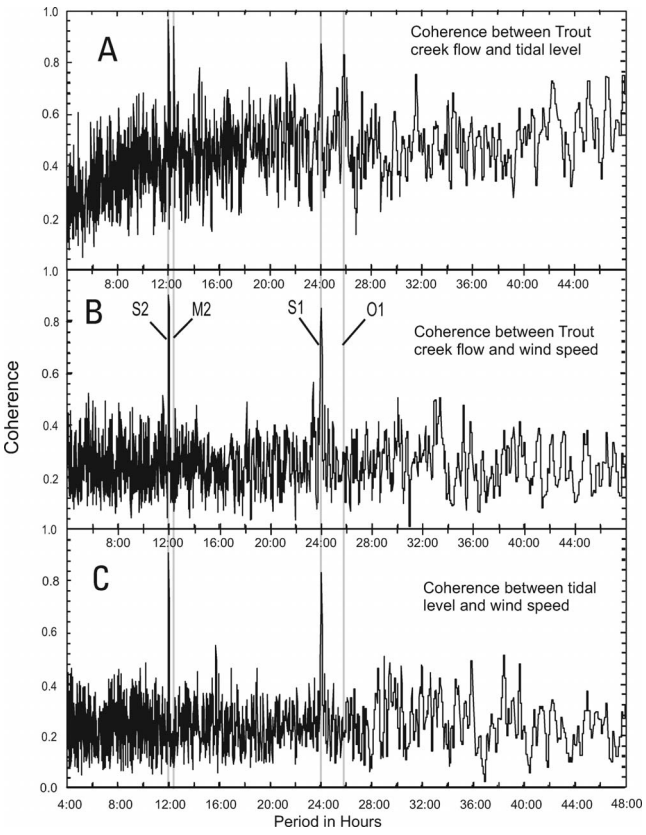

Figure 5. Coherence of tidal water-levels, wind speed, and measured Trout Creek flows.

(and rainfall and inland boundaries shown in Figure 4) generally are negligible on the fluctuations in flow at Trout Creek for periods of less than 48 hours.

Wind accounts for most Trout Creek flow fluctuations on 12- and 24-hour frequencies. Tidal boundaries account for nearly all fluctuations on 12-hour, 25-minute and 25-hour, 49-minute frequencies, which correspond to the M2 and O1 tidal components, respectively.

The calibrated model represents the 12- and 24-hour components of flow fluctuations at Trout Creek better than the 12-hour, 25-minute and 25-hour, 49-minute components, which, when combined with conclusion 2, indicates that wind effects on Trout Creek flow are represented better than tidal water-level boundary effects.

These results indicate that the measurement of tidal boundary water-level fluctuation effects may be the primary source of error for higher frequency discharge fluctuations at Trout Creek—a major coastal outflow point.

Harmonic Analysis of Experimental Simulations

The spectral amplitudes shown in Figures 3 and 4 are not the most accurate representations of the actual spectral power. The widths of different peaks vary, so the value of the maximum value is not a complete measure of the total power associated with a specific frequency. A more accurate method

Table 3. *Spectral power of forcing functions at principal tidal periods (determined from harmonic analysis).*

Forcing Function or Discharge	Spectral Power in Original Units (Dashes Indicate Negligible Power)			
	12-h, 25-min Component (M2)	25-h, 49-min Component (O1)	12-h Component (S2)	24-h Component (S1)
Evapotranspiration (cm/d)	—	—	—	0.31
Wind (m/s)	—	—	—	0.822
Tidal boundary (cm)	0.21	0.22	0.25	0.30
Measured Trout Creek discharge (m^3/s)	0.787	1.048	0.581	1.047
Computed Trout Creek discharge (m^3/s)	0.519	0.805	0.396	0.453

for determining the spectral amplitude associated with a specific frequency is to use a least-squares method to fit a cosine function of the desired frequency to the data. This "harmonic analysis" matches the amplitude and phase to minimize the least-square errors. The amplitude is expressed in the original units of the data. To evaluate the magnitudes of spectral components in the model forcing functions, the harmonic analysis was used. Neither rainfall nor the inland boundaries produced significant components. The computed evapotranspiration spectral magnitude at the 24-hour (S1) frequency is 0.31 cm/d. The wind velocity has a 12-hour (S2) component of 0.219 m/s and a 24-hour (S1) component of 0.822 m/s. These results are shown in Table 3.

The harmonic analysis was also applied to the water-level measurements used for the tidal boundary and both the measured and computed discharges at Trout Creek. These results are also shown in Table 3. Note that for the water-level measurements used for the tidal boundary, the 12-hour, 25-minute component (M2) had an amplitude of 0.21 cm and the 25-hour, 49-minute component (O1) had an amplitude of 0.22 cm. The field measurements of water level, made to the nearest 0.30 cm, has an average error of 0.30/4 = 0.075 cm, so the M2 and O1 tidal components are only about three times larger than the average measurement error.

Numerical Model Uncertainty Considerations

When evaluating the effect of errors in field measurements on the model's flow spectra, the potential effect of errors inherent to the numerical model must be considered. In SWAIN *et al.* (2004), an uncertainty analysis was performed on the SICS model by individually perturbing the model input parameters and observing the variability in the model-computed coastal flows. Of the eight types of parameters that were perturbed, the highest sensitivity was related to the frictional resistance of the coastal creeks. Changing the coastal creek resistance by 50% induced mean absolute differences in flow at Trout Creek from 3.6 to 4.6 m^3/s. However, a temporally constant parameter such as frictional resistance affects the amplitudes of flow fluctuations at all frequencies so it cannot account for the disparities in the ability to represent different frequency spectral powers. This is true of most of the numerical model parameters analyzed, except for rainfall, evapotranspiration, wind, inland boundaries, tidal boundaries, and the effects of salinity variations on density. All these are part of the spectral analysis in the "Spectral Analysis of Experimental Simulations" section of this paper, except for the salinity variation effects. However, the sensitivity test in SWAIN *et al.* (2004) indicated that totally neglecting the effects of salinity variations on density only induced a mean absolute difference in flow at Trout Creek of 0.66 m^3/s.

The temporally varying parameter that indicated the highest sensitivity was in fact the tidal boundary. Changing the tidal boundary by 0.1 m induced mean absolute differences in flow at Trout Creek from 1.1 to 2.6 m^3/s. To examine the effects of temporal fluctuations in tide, we added a sinusoidal function with an amplitude of 0.3 m to the western tidal boundary. This produced a mean absolute difference in flow at Trout Creek of 4.6 m^3/s. A similar hypothetical tide function is subjected to spectral analysis in the "Comparison to Numerical Models" section of this paper.

ERROR PROPAGATION FORMULATION

The limitations associated with field measurements are one possible source of errors in the representation of tidal boundary levels in the numerical model. Field water-level measurements are made by a continuous recorder to the nearest 0.30 cm. Each water-level measurement can have a maximum error of ± 0.15 cm because it is reported to the nearest gauge increment. For a large data set where the water level varies over a range substantially more than one water-level gauge increment, the error is uniformly distributed over the range from -0.15 to $+0.15$ cm.

POTTER and WALKER (1981, 1985) discuss stage–discharge relationships used for peak flow determination. They found that errors in peak flow measurements are often larger than the usual errors in the stage–discharge rating. This has important implications in flood frequency analysis. These cases differ from the coastal situation in this paper in that the peak flow case involves a large stage variation with a fixed stage–discharge relationship. Our coastal situation has a very low water gradient, no fixed stage–discharge relationship, and a strong dependency of discharge on stage gradient. Thus the error characteristics are different with the effect of stage-measurement errors on the stage gradient being the important factor.

Equation Derivation

A formulation that relates the magnitude of the water-level gauge errors to discharge errors is needed to determine if the spectral magnitude errors are likely due to measurement errors. Including terms for the related water-level measurement error and computed discharge error in the steady-state approximation of the discharge-gradient relation yields:

$$Q_i + e_{qi} = \Gamma\sqrt{\Delta z_i + e_{zi}} \tag{4}$$

where Q_i is the discharge at measurement i, e_{qi} is the error in discharge computed at measurement i resulting from errors in water-level measurement, Γ is the proportionality between discharge and the square root of water-level difference, Δz_i is the water-level difference through the creek between some defined upstream and downstream locations (the down-

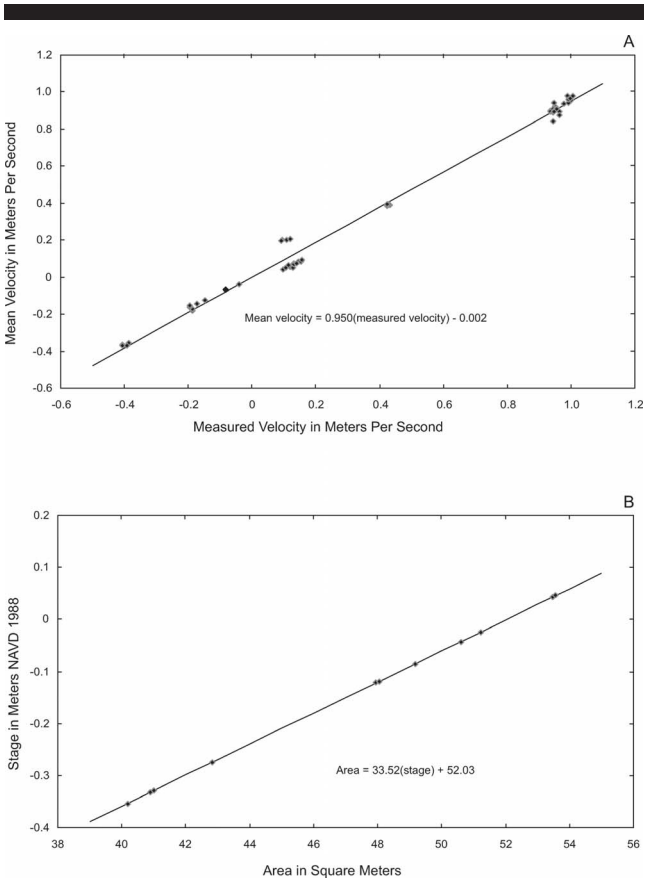

Figure 6. Velocity and stage-area ratings for Trout Creek discharge station.

stream water-level defined by the tidal boundary), and e_{zi} is the error in water-level measurement at measurement i. Equation (4) is for steady one-dimensional flow. The creek flow is represented as one-dimensional in the numerical model also, even though the rest of the surface-water computations are two dimensional. Equation (4) is to be used to represent the net error in discharge over the period of record. Using the steady flow equation assumes that inertial effects are negligible for the long-term average—a reasonable assumption. The only induced error in Equation (4) is in downstream stage measurement, e_{zi}. It should be noted that, in the following application, the discharge error e_{qi} is equated to the errors in spectral power: the errors in the temporal fluctuation magnitude. Because these frequency fluctuations are due to tide, the error in downstream stage measurement e_{zi} is the relevant error, not any inherent errors in Γ or upstream stage.

Equation (4) does not include a dependency on water depth. The information from the field discharge measurement site can be used to determine if this is a reasonable approximation. In the development of the Trout Creek station rating curve that relates measured velocity to mean velocity, shown in Figure 6A, the regression analysis did not require water depth as a significant variable relative to the measured velocity variation for a close fit (HITTLE, PATINO, and ZUCKER, 2001). In addition, a basic statistical analysis of the water-level data at the Trout Creek station shows a standard deviation of 0.101 m; only 6.7% of the average depth of approximately 1.5 m. Figure 6B shows the relationship between stage and cross-sectional area at the Trout Creek station, which is nearly linear because of the steep side slopes. Using the developed rating equation shown in Figure 6B, a 0.101 m change in stage only yields a 3.4 m^2 change in cross-sectional area, about a 7% change. Given that the discharge regularly changes direction because of the gradient, a much larger effect than that of cross-sectional area change, it is reasonable to not include a depth dependency in Equation (4).

If Manning's equation is related to Equation (4), the proportionality is:

$$\Gamma = \frac{1}{\eta}\frac{AR^{2/3}}{L^{1/2}} \tag{5}$$

where η is Manning's friction factor, A is the cross-sectional area of the creek, R is the hydraulic radius, and L is the length of the creek. Stage-measurement errors of interest would translate to depth errors in the A and R terms in Equation (5). Γ is proportional, through A and R, to depth to the 5/3 power. The stage measurement error is less than 0.0015 m, and the mean depth is 1.5 m. So even if the error was biased at its maximum value, the error in Γ would be $(0.0015/1.5)^{5/3} = 0.001\%$. So there is no error term associated with Γ in Equation (4).

In Equation (4), the head-difference term with measurement error, $\Delta z_i + e_{zi}$, can be called the measured head difference, $\Delta\hat{z}$. Making this replacement and setting $Q_i = \Gamma\sqrt{\Delta z_i}$, Equation (4) can be rearranged as follows:

$$e_{qi} = \Gamma\left(\sqrt{\Delta\hat{z}_i} - \sqrt{\Delta z_i}\right). \tag{6}$$

Taking the mean of both sides and defining e_q as the mean of the flow errors e_{qi}:

$$e_q = \Gamma\left(\overline{\sqrt{\Delta\hat{z}_i}} - \overline{\sqrt{\Delta z_i}}\right) \tag{7}$$

where the overbar indicates the mean.

The error e_{zi} occurs because of the distance of the actual water level from an increment of the water-level gauge. Figure 7 shows the relationship of the upstream and downstream water levels, the water-level gradient between them, the downstream water-level gauge increment, and the measurement error e_{zi}. The points on the measurement error scale upon which the downstream stage falls in Figure 7 depend only on the proximity of the downstream stage to a measurement increment. The measurement error e_{zi} ranges from -0.15 cm to $+0.15$ cm with the particular value not corresponding to any particular water-level gradient. A high water-level gradient may have a downstream stage with either a high or low measurement error, as might a low water-level gradient. So Figure 7 indicates that when the downstream water level varies over a number of these increments during the multiyear dataset, the error e_{zi} does not correlate to any particular water-level gradient or the magnitude of the water-level difference Δz_i. So assuming Δz_i and e_{zi} are uncorrelated, and $\Delta\hat{z} = \Delta z_i + e_{zi}$, then $\Delta z_i = \overline{\Delta\hat{z}_i}$ and Equation (7) becomes:

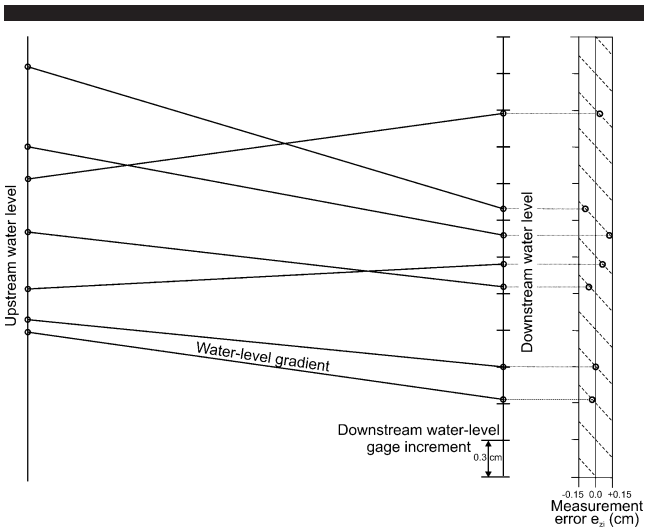

Figure 7. Schematic diagram showing the lack of correlation between water-level gradients and measurement errors at a downstream gauge with discrete measurement increments.

$$e_q = \Gamma\left(\overline{\sqrt{\Delta\hat{z}_i}} - \sqrt{\overline{\Delta\hat{z}_i}}\right). \quad (8)$$

When higher- order terms in a Taylor series are neglected, a statistical property of expected values (means) is:

$$\overline{f(x)} - f(\bar{x}) = \frac{1}{2}f''(\bar{x})\mathrm{VAR}[x] \quad (9)$$

where VAR[x] is the variance of x. With $f(x) = \sqrt{x}$ and $x = \Delta\hat{z}_i$, Equation (9) can be put into the right-hand side of Equation (8) to yield:

$$e_q = \Gamma\left\{-\frac{1}{8}\left(\overline{\Delta\hat{z}_i}\right)^{-3/2}\mathrm{VAR}[\Delta\hat{z}_i]\right\}. \quad (10)$$

With $(\overline{\Delta\hat{z}_i})^{-3/2} = \overline{(\Delta z_i)^{-3/2}} = \overline{1/\sqrt{\Delta\hat{z}_i}^3}$ and $\mathrm{VAR}[\Delta\hat{z}_i] = \overline{e_{zi}^2}$, Equation (10) becomes:

$$e_q = \frac{-\Gamma}{8}\overline{\left(\frac{1}{\sqrt{\Delta z_i}^3}\right)}\overline{e_{zi}^2}. \quad (11)$$

With $\sqrt{\Delta\hat{z}_i} = Q_i/\Gamma$, Equation (11) becomes:

$$e_q = \frac{-\Gamma^4}{8}\overline{\left(\frac{1}{Q_i^3}\right)}\overline{e_{zi}^2}. \quad (12)$$

Error Evaluation

To evaluate the induced error in computed flow e_q, the three independent variables on the right-hand side of Equation (12) must be evaluated. The value of Γ could be computed with Equation (5) using estimates of η, A, R, and L; however, a less approximate method is available. If Manning's equation applies, the equation $\Gamma = Q/\sqrt{\Delta z}$ is true not only when Q and Δz are fixed values, but also when Q is a flow fluctuation and Δz is the corresponding head difference fluctuation. The fluctuations in these values at certain frequencies are expressed by their spectral amplitudes. Because it has been shown that the M2 and O1 flow fluctuations are due to the tidal water-level boundary, the spectral amplitude of the tidal boundary can be considered a close approximation of the spectral amplitude of the head difference Δz. Therefore, the numerical model results can be used to estimate Γ at a given tidal frequency by using the amplitude of the computed discharge spectrum as Q and the amplitude of the tidal boundary water-level spectrum as Δz in the equation $\Gamma = Q/\sqrt{\Delta z}$. For the purposes of the calculations, Γ can be defined to correspond to Q (hence e_q) in cubic meters per second and Δz (hence e_{zi}) in centimeters.

As shown in Table 3, a harmonic analysis of the tidal boundary water-level fluctuations yielded an M2 amplitude of 0.21 cm and an O1 amplitude of 0.22 cm. The harmonic analysis of the computed discharge data at Trout Creek indicates that the M2 and O1 components have respective amplitudes of 0.519 and 0.805 m^3/s, yielding Γ values of 1.132 and 1.715. These Γ values are only appropriate for discharge measured in cubic meters per second and water level measured in centimeters. Additionally, using the numerical model results for this purpose also assumes that the hydrodynamic relations are represented accurately in the model. As a reasonable estimate, an average value of $\Gamma = 1.42$ was used.

The independent variable $\overline{1/Q_i^3}$ in Equation (12) was evaluated using the measured discharge data. The quantity $1/Q_i^3$ was summed up over the entire 1996–2002 period and averaged for a resulting value of 58.74 s^3/m^9. The final independent variable in Equation 12, $\overline{e_{zi}^2}$, was evaluated for a uniform distribution between -0.15 and $+0.15$ cm (Figure 7). Because the mean of the uniform distribution is zero, $\overline{e_{zi}^2}$ is equal to the variance of the distribution, which is (range of distribution)^2/12 = 0.30^2/12 = 0.0075 cm^2. Using these values, Equation (12) yields an error in creek discharge, e_q, induced by measurement error at the tidal water-level gauge of -0.226 m^3/s. The negative sign indicates that the error reduces the magnitude of the flow fluctuations. This is supported by Figure 3, which also indicates the error tends to reduce the flow fluctuation.

Statistical Test of Error Significance

To determine if the model-computed discharge error due to measurement error at the tide gauge e_q is significant relative to inherent errors in the field-computed discharge measurements used for comparison, we performed a statistical test. The flow velocity at Trout Creek (Hittle, Patino, and Zucker, 2001) is measured by an acoustic doppler velocity meter (ADVM), which has a rated standard error of 0.5 cm/s or 0.005 m/s. This measured velocity is converted to a mean velocity through a rating curve, developed from a number of acoustic velocity measurements, which has a standard error of 0.037 m/s. With these two errors added to a 0.042 m/s velocity error, and a creek cross-sectional area of approximately 52 m^2, the standard error in the field-computed discharge is about $\sigma = 2.2$ m^3/s. With a large data set collected at 15-minute intervals for 7 years, a total number of data points $n = 245{,}472$, random errors can be represented as normally distributed with a mean $y = 0$. A two-tailed statistical test

can be performed for the null hypothesis that the mean field-computed error equals the tide-gauge induced error $e_q = -0.226$ m³/s, using the test statistic $Z = |y - e_q|/(\sigma/\sqrt{n}) = 50.9$. For a 99% confidence level in a two-tailed test, Z would have to be larger than $Z_{0.01/2} = 2.575$ to reject the null hypothesis that the field computed discharge error equals the model-computed discharge error due to measurement error at the tide gauge e_q. Because 50.9 is much larger than 2.575, we reject the null hypothesis and state that the model-computed discharge error due to measurement error at the tide gauge e_q is significant relative to inherent errors in the field-computed discharge measurements used for comparison.

Comparison to Numerical Models

A comparison of the Equation (12) results with the actual error induced in the model is informative; the value of $e_q = -0.226$ m³/s is 28.7% of the M2 amplitude of measured discharge fluctuation in Table 3 and 21.6% of the O1 amplitude. This means that the M2 and O1 components would be reduced to 71.3% and 78.4%, respectively. The actual reductions in discharge fluctuation amplitude in the model is determined from Table 3 by (computed Trout Creek discharge)/(measured Trout Creek discharge) × 100%, yielding 65.9% for the M2 component and 76.8% for the O1 component. Equation (12) represents discharge errors associated with water-level gauge resolution consistent in magnitude and sign to the errors in the underestimation of discharge spectral power seen in the numerical model. This indicates that the lack of sufficient discharge fluctuation magnitude in the numerical model representation of tidal components can be largely due to the resolution of the water-level gauge used to create the tidal boundary in the model.

To further test the hypothesis that the discharge fluctuation errors observed can be explained by the measurement errors at the tidal boundary, we created two simulations with a synthetic 25-cm amplitude S2 tide added to the boundary. This is a significantly larger tidal range than the actual Florida Bay values. In one simulation, only the tide is added. In the second simulation, along with the tide, a 0.087-cm error value is added that alternates positive and negative. This error value produces the same variance (0.0075 cm²) as the measurement error assumed for the tidal gauge. The amplitude of the S2 component of the discharge values at Trout Creek from these two runs are then evaluated with the harmonic analysis. The simulation without the error has a discharge S2 amplitude of 21.850 m³/s and the simulation with the error has a discharge S2 amplitude of 21.680 m³/s. This difference of −0.180 m³/s compares very well with the equation-predicted error of −0.226 m³/s. This analysis also demonstrates the analysis under conditions with a higher amplitude tide (25 cm *vs.* 0.25 cm). Of course the discharge error is a smaller percentage of the total discharge fluctuation under these conditions.

Comparison of the numerical model errors in representing flow fluctuation spectral power with those predicted by Equation (12) indicates the equation's appropriateness. Equation (12) has been shown to: (1) predict the error magnitude that has been attributed by the model to tidal stage errors; (2) predict the error magnitude that was artificially induced into the numerical model by adding a tidal signal; and (3) produce errors that are significant in magnitude relative to other errors.

SUMMARY AND CONCLUSIONS

A combined numerical model–spectral analysis can be used to help delineate the separate forcing functions that affect coastal outflows in a combined wetland–bay system and quantify sources of errors in boundary conditions. An application to the southeastern Everglades–northeastern Florida Bay numerical model initially involved computing the power spectrum of the simulated flows at Trout Creek (a coastal site) and comparing this with the spectrum of measured flow at Trout Creek. This comparison identified four dominant power frequencies, corresponding to S1, S2, M2, and O1 tidal periods. The model appeared to reproduce the magnitudes of the S1 and S2 components better than the M2 and O1 components.

A steady-base version of the model was created with all time-varying forcing functions (rain, evapotranspiration, wind, and inland and tidal boundaries) set to averaged values. Each forcing function was varied individually to delineate its effects. Results indicate that rain, evapotranspiration, and inland boundaries each had little or no effect on the four dominant power frequencies. Wind had a predominant effect on the frequencies corresponding to the S1 and S2 components, and tidal boundaries were the sole generator of the M2 and O1 components. Because the M2 and O1 components of Trout Creek flow were the least well represented, it was concluded that the effect of tidal boundaries is probably not being represented as well as wind-forcing effects in the model. An analytical equation was developed, relating the error in water-level measurements to the induced error in model-produced flow fluctuations. The water-level errors were assumed to have the statistical distribution of the errors in a water-level gauge associated with the resolution increments. The errors in computed discharge fluctuation magnitude derived from the analytical equation were similar to those seen in the discharge computed by the numerical model.

To further investigate the validity of the analytic equation and the possible effect of tidal measurement error, we performed additional numerical model simulations with an artificial tidal signature and a perturbation similar in magnitude to the error from the tidal water-level gauge. Two model simulations, with and without the error perturbation, indicated a difference in spectral power similar to that predicted by the analytic equation and that seen in the comparison of the calibrated model to the field-measured data.

Some of the deficiencies in the numerical model representation of the M2 and O1 tidal components of discharge through Trout Creek can be explained by the limits in resolution of the water-level gauges used to define the tidal model boundary. This conclusion is based on: (1) the spectral analysis of the modified numerical model simulations, (2) the analytical equation expressing water-level gauge-error effects, and (3) the numerical model simulations with and without the artificial tidal error. Additionally, the wind-induced components of discharge seem to be better represented than the tidally induced components of

discharge. The sensitivity of the numerical model representation of discharge volumes to small errors in boundary water levels has been known intuitively, but the current analysis quantifies the problem more definitively. The combined use of a numerical model and spectral analysis allows for more extensive analyses. A numerical model that has been sufficiently developed and calibrated to properly represent the controlling processes can be used to delineate individual forcing-function effects that could not be determined otherwise. The spectral analysis can then be used to locate and quantify characteristic frequency responses and relate them to their inducing forcing functions. The current effort shows how it is possible to use spectral analysis to locate and quantify error sources and gain a better understanding of the dynamics of the hydrologic area modeled.

NOTATION

A	cross-sectional area of the creek.
$C_x(\tau)$	covariance of quantity x at a time lag of τ.
e_{qi}	error in discharge computed at measurement i.
e_{zi}	error in water-level measurement at measurement i.
i	imaginary number $\sqrt{-1}$.
L	length of the creek.
n	number of segment in spectral analysis.
Q_i	discharge at measurement i.
R	hydraulic radius.
$S_{xx}(\omega)$	spectrum of quantity $x(t)$ at a time frequency of ω.
t	time.
T	total time analyzed.
$\bar{x}$	time-averaged value of quantity x.
$\bar{y}$	arithmetic mean.
Z	two-tailed test statistic.
Δz_i	water-level difference through the creek at measurement i.
$\Delta\hat{z}_i$	water-level difference with measurement error; equals $\Delta z_i + e_{zi}$.
Γ	proportionality between discharge and the square root of water-level difference.
η	Manning's friction factor.
σ	standard error.
χ^2	chi-squared parameter.

ACKNOWLEDGMENTS

The authors would like to thank the Priority Ecosystem Studies (PES) program for funding the development of the numerical model and further analysis used in this report. Thanks also to the U.S. Geological Survey personnel and others who contributed to the development of the numerical model and the necessary data.

LITERATURE CITED

BENDAT, J.S. and PIERSOL, A.G., 2000. *Random Data, Analysis and Measurement Procedures,* 3rd edition. New York: John Wiley, 594p.

COOLEY, J.W. and TUKEY, J.W., 1965. An algorithm for the machine calculation of complex Fourier series. *Mathematics of Computation,* 19, 297–301.

FERRANTE, M. and YEH, T.-C.J., 1999. Head and flux variability in heterogeneous unsaturated soils under transient flow conditions. *Water Resources Research,* 35(4), 1471–1479.

GERMAN, E.R., 2000. Regional Evaluation of Evapotranspiration in the Everglades. U.S. Geological Survey Water-Resources Investigations Report 00-4217, 48p.

GUO, W. and LANGEVIN, C.D., 2002. User's guide to SEAWAT: a computer program for simulation of three-dimensional variable-density ground-water flow. *In: U.S. Geological Survey Techniques of Water-Resources Investigations* Book 6, Chap. A7, 77p.

HITTLE, C.D., 2000. Quantity, timing, and distribution of freshwater flows into northeastern Florida Bay. *U.S. Geological Survey Program on the South Florida Ecosystem: 2000 Proceedings.* U.S. Geological Survey Open-File Report 00-449.

HITTLE, C.D.; PATINO, E., and ZUCKER, M., 2001. Freshwater Flow from Estuarine Creeks into Northeastern Florida Bay. U.S. Geological Survey Water-Resources Investigations Report 01-4164, 32p.

LANGEVIN, C.D.; SWAIN, E.D., and WOLFERT, M.A., 2005. Simulation of integrated surface-water/ground-water flow and salinity for a coastal wetland and adjacent estuary. *Journal of Hydrology,* 314, 212–234.

LUMLEY, J.L. and PANOFSKY, H.A., 1964. *The Structure of Atmospheric Turbulence.* New York: John Wiley.

POTTER, K.W. and WALKER, J.F., 1981. A model of discontinuous measurement error and its effects on the probability distribution of flood discharge measurements. *Water Resources Research,* 17(5), 1505–1509.

POTTER, K.W. and WALKER, J.F., 1985. An empirical study of flood measurement error. *Water Resources Research,* 21(3), 403–406.

RETTEMEIER, K.; BERGEN, O.; VAN LINN, A., and KONGETER, J., 2001. Numerical modeling of turbulence in lakes and reservoirs with large eddy simulation technique: 21st century: the new era for hydraulic research and its applications. *In: XXIX IAHR Congress, September 16–21, 2001 (*Beijing, China, Tsinghua University Press), pp. 545–552.

SCHAFFRANEK, R.W., 2004. A model for simulation of surface-water integrated flow and transport in two dimensions: SWIFT2D user's manual. *U.S. Geological Survey Techniques and Methods,* Book 6, Chap. 1, 115p.

SCHAFFRANEK, R.W.; RUHL, H.A., and HANSLER, M.E., 1999. An overview of the Southern Inland and Coastal System Project of the U.S. Geological Survey South Florida Ecosystem Program. *In: Proceedings of the 3rd International Symposium on Ecohydraulics* (Salt Lake City, July 13–16, 1999).

SCHUREMAN, P., 1976. *Manual of Harmonic Analysis and Prediction of Tides.* U.S. Dept. of Commerce, Coast and Geodetic Survey, Special Publ. No 98, Washington D.C.: U.S. Government Printing Office.

SHIH, D.C.-F., 2002. Identification of phase propagation of water level in tidal river by spectral analysis. *Stochastic Environmental Research and Risk Assessment,* 16(6), 449–463.

SHIH, D.C.-F., 2004. Uncertainty analysis: one-dimensional radioactive nuclide transport in a single fractured media. *Stochastic Environmental Research and Risk Assessment,* 18, 198–204.

SHIH, D.C.-F.; LEE, C.-D.; CHIOU, K.-F.; TSAI, S.-M.; TSAI, C.-H., and TSAI, C.-T., 2000. Spectral analysis of tidal fluctuations in ground water level. *Journal of the American Water Resources Association,* 36(5), 1087–1099.

SHIH, D.C.-F. and LIN, G.F., 2002. Spectral analysis of water level in aquifers. *Stochastic Environmental Research and Risk Assessment,* 16(5), 374–398.

SWAIN, E.D. and CHIN, D.A., 2003. An analytical formulation of two-dimensional groundwater dispersion induced by surficial recharge variability. *Water Resources Research,* 39(9), 1271–1278.

SWAIN, E.D.; WOLFERT, M.A.; BALES, J.D., and GOODWIN, C.R., 2004. Two-Dimensional Hydrodynamic Simulation of Surface-Water Flow and Transport to Florida Bay through the Southern Inland and Coastal Systems (SICS). U.S. Geological Survey Water-Resources Investigations Report 03-4287, 62p.